



GTT-Technologies
Kaiserstraße 103
52134 Herzogenrath, Germany
Phone: +49-(0)2407-59533
Fax: +49-(0)2407-59661
E-mail: info@gtt-technologies.de

GTOx Version 17 Documentation

Table of contents

Introduction.....	1
Database content overview	2
Thermophysical modelling	5
Viscosity.....	5
Density	5
Application examples.....	6
De-phosphorisation of steels in the BOF process	6
Refractory applications.....	8
Distribution of Vanadium.....	10
Slag formation, fouling, and condensation from coal/biomass/waste gasification and combustion	11
Optimization of slag mobility in entrained flow gasifiers	14
Assessment examples	16
ZnO-P ₂ O ₅	16
CaO-ZnO-P ₂ O ₅	19
Al ₂ O ₃ -Li ₂ O-MgO.....	21
Viscosity modelling.....	22
Density modelling.....	25
Database compatibility.....	28
Phases	29
Solid solution phases	29
Solid stoichiometric compounds	29
Liquid slag	29
Liquid sulphate.....	29
Liquid metal	30
What is new in version 17?.....	31
Contact	33

Introduction

The present GTOx database contains thermodynamic data covering binary, ternary and quaternary sub-systems among the following components:

**Al₂O₃-Al₂S₃-CaO-CaF₂-CaS-Cr₂O₃-CrS-CuO-Cu₂O-FeO-Fe₂O₃-FeS-Li₂O-MgO-
MgS-MnO-Mn₂O₃-MnS-K₂O-K₂S-Na₂O-Na₂S-NiO-NiS-P₂O₅-SO₃-SiO₂-SrO-TiO₂-
Ti₂O₃-V₂O₃-V₂O₅-ZnO**

Information concerning the sub-systems already assessed in the database is given in appropriate charts in the [next chapter](#). For calculations in higher order systems the data of the subsystems are extrapolated. The database is the result of an ongoing thermochemical (Gibbs energy) and thermophysical (density, viscosity) assessment project to obtain the data for the respective phases in each system. These assessments have been carried out in the framework of past and ongoing projects sponsored by German as well as European funding agencies in close collaboration with Forschungszentrum Jülich (IEK-2)¹.

Recently, the scope of the database has been expanded in order to additionally cover thermophysical properties of oxides. The most relevant properties are the viscosities of slag melts, however, some work was also devoted to modelling the density, and thus the molar volume, of such melts. The density database will also be extended to the solid phases, thus enabling the linking of the two properties viscosity and volume in the modelling of viscosities in the solid-liquid range.

For representative cases of data assessments as well as applications of the data see the Chapters [Assessment examples](#) and [Application examples](#). For users with a direct need for phase diagrams calculated using the present database, GTT additionally offers access to its Slag Atlas, i.e. the full collection of all phases diagrams calculated during the thermodynamic assessments. Please [contact us](#). For those readers who are interested in the recent changes and additions to this version, please check the Chapter: [What is new in version 17?](#).

¹ Forschungszentrum Jülich GmbH - Institut für Energie- und Klimaforschung, Structure and Function of Materials (IEK-2), PD Dr. Michael Müller

Database content overview

The present GTOx database consists of Gibbs energies for the melt phases Slag, Liquid Metal and Liquid Sulphate, as well as **153 solid solution phases** and **821 stoichiometric phases**. The figures (1-4) below indicate systems which have been assessed. Note that an O or R in a green square indicates that the data are mainly valid for (O)xidizing respectively (R)educing conditions. Such a distinction has to be made for metals with multiple valences (Fe, Mn, Cu, Cr, V, Ti). If neither O nor R is indicated for these metals, the systems are assessed for both conditions.

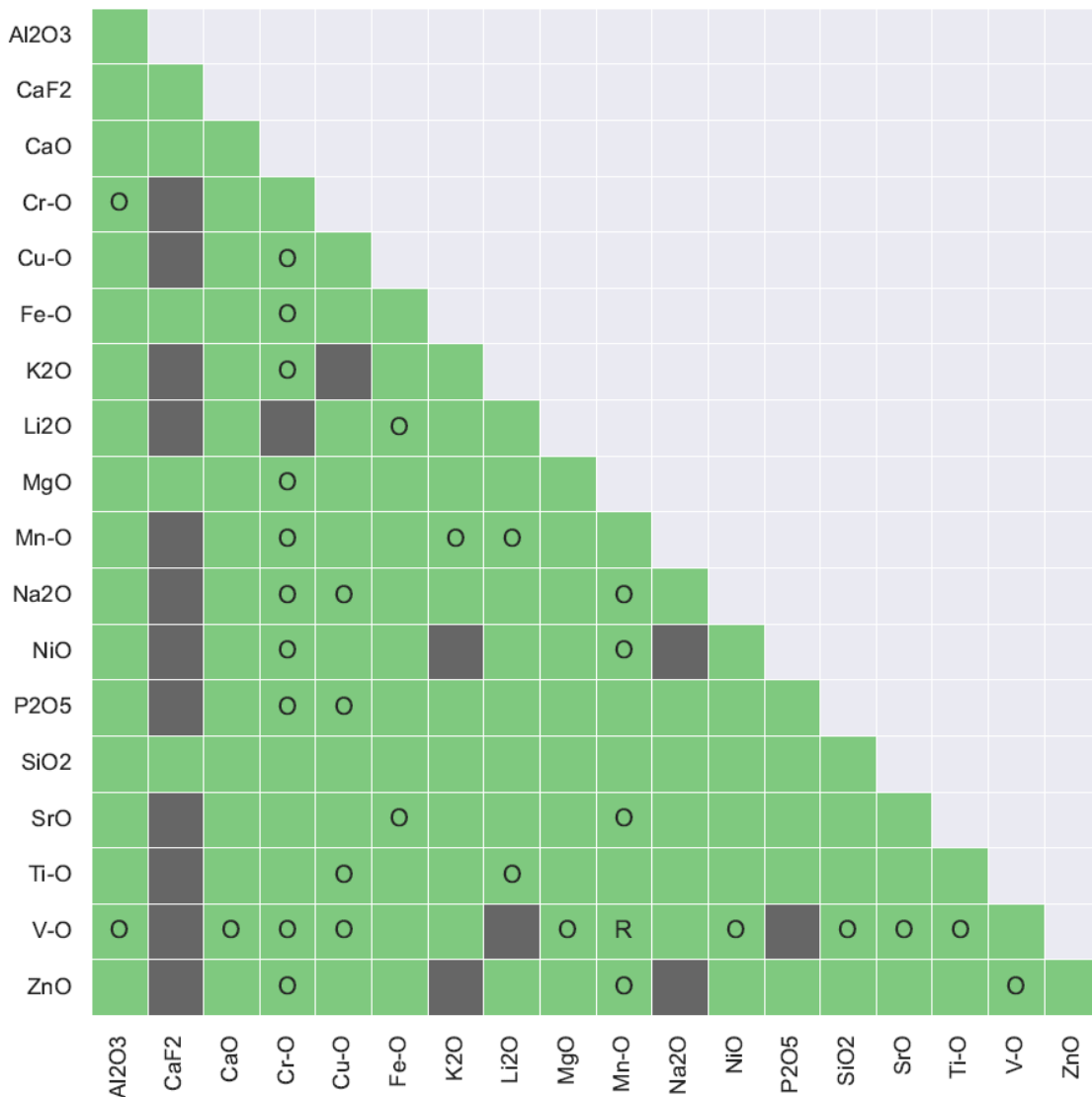


Figure 1: Assessed (green) binary oxide systems in the GTOx database. O and R denote systems for which the data is mainly valid for oxidizing and reducing conditions, respectively.



Figure 2: Assessed (green) sulfide-containing (left) or sulphate-containing (right) binary systems in the GTOx database. O denotes systems for which the data is mainly valid for oxidizing conditions.

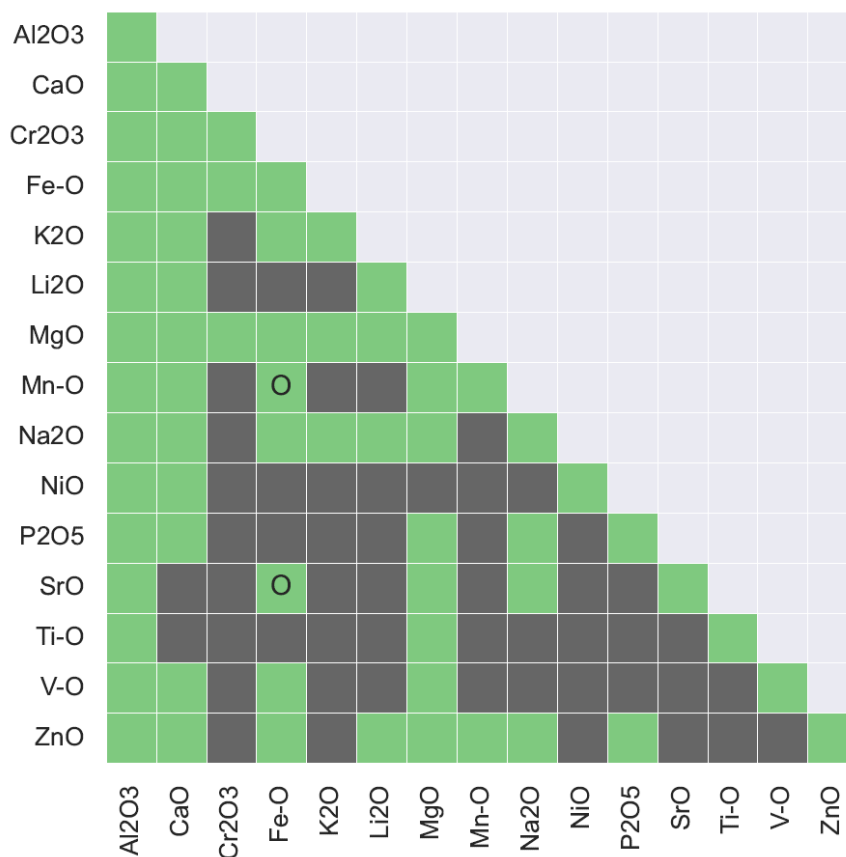


Figure 3: Assessed (green) SiO₂-containing ternary systems in the GTOx database. O denotes systems for which the data is mainly valid for oxidizing conditions.

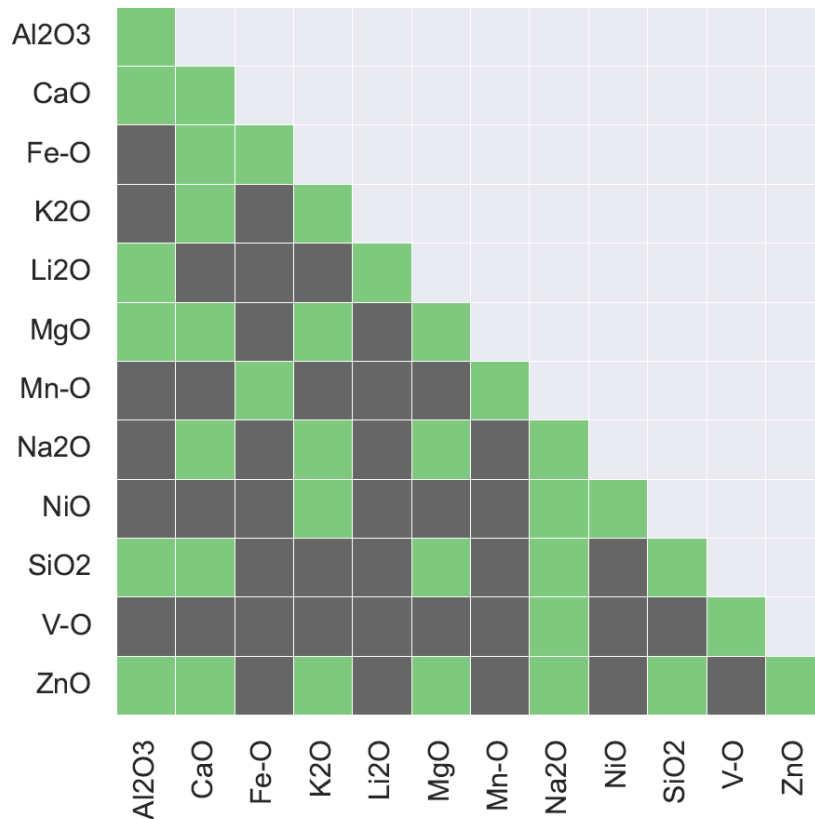


Figure 4: Assessed (green) P_2O_5 -containing ternary systems in the GTOx database.

Figure 3 shows the ternary systems containing SiO_2 . As can be seen, most combinations usually observed in ferrous and non-ferrous metallurgy, cement making and combustion ashes (systems with main components from SiO_2 - Al_2O_3 - CaO - FeO_x - MgO - MnO_x) are covered.

Figure 4 shows the ternary systems containing P_2O_5 . Recently, there has been strong interest in P_2O_5 -containing systems because of the focus on Phosphorous recovery from, for instance, sewage sludge, but also because many iron ores processed in East Asia in particular contain large amounts of P_2O_5 . Furthermore, P_2O_5 is an important component of biomass ashes. To describe these applications, most combinations usually observed – such as systems with main components from SiO_2 - Al_2O_3 - CaO - FeO_x - K_2O - MgO - Na_2O – are covered.

Thermophysical modelling

Viscosity

A viscosity model for fully liquid (i.e. also supercooled) melts has been developed, where the viscosity is directly correlated to the structure of oxide melts, and the melt structure in turn is described based on the thermodynamic description applied, i.e. using the modified non-ideal associate species model. The present viscosity model covers the system **SiO₂-Al₂O₃-CaO-MgO-Na₂O-K₂O-FeO_x** using a set of model parameters for the viscosity which all have a clear physical meaning.

A corresponding *viscosity calculator* has been developed based on [ChemSheet](#). A screenshot of the user interface is shown below in Figure 5. Note that a valid ChemSheet license is required to use the viscosity calculator.

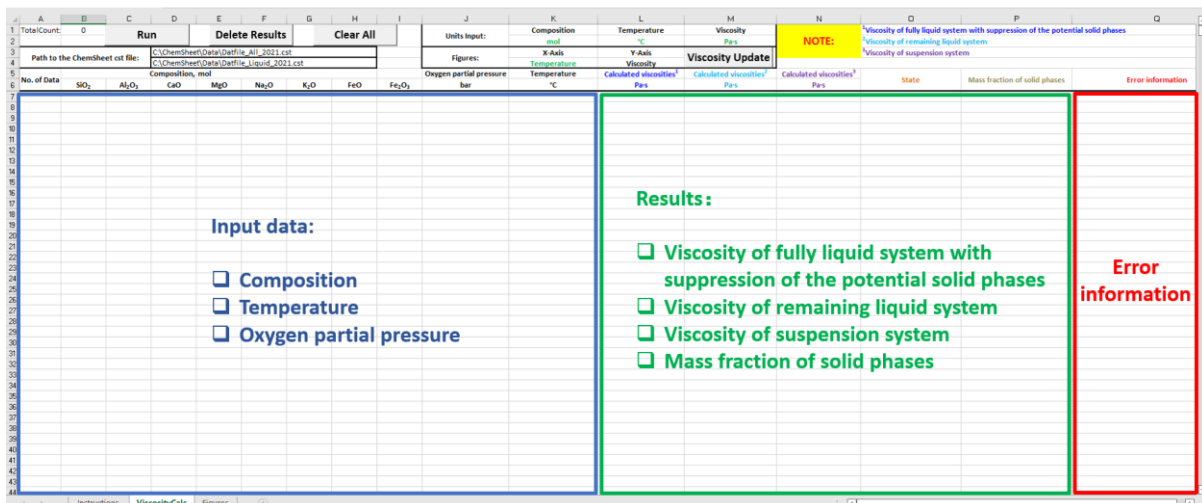


Figure 5: Screenshot of the GTOx-based viscosity calculator in ChemSheet.

Density

A density model for fully liquid (i.e. also supercooled) melts has been developed covering the system **SiO₂-Al₂O₃-CaO-MgO-Na₂O-K₂O**. Note that densities of solid phases are not yet part of the release but already under development.

Application examples

De-phosphorisation of steels in the BOF process

In the basic oxygen steelmaking (BOF) process, the accurate control of phosphorous removal up to ultra-low values is very important to ensure a high quality of the end product. This has proven to be associated with several challenges, leading to a preferred usage of high-priced low-P iron ores. Thus, in the scope of the European RFCS project BOFdePhos (RFSR-CT-2014-00005), important thermodynamic and kinetic aspects of the dephosphorisation reaction such as the effect of solid phases on phosphorous distribution and lime dissolution in a foamy slag were investigated.

It was found that BOF slags contain solid oxides during a large period of the blow and, in most cases, also at the end of blow. The type and amount of solid phases is strongly affected by temperature and minor oxides content such as MgO-, MnO- and Al₂O₃-content. The consideration of solid phases formation in the slag, especially the P-dissolving C₂S-C₃P solid solution, is crucial for a successful modelling and control of de-phosphorisation. However, most of the phosphorous distribution equations available in the literature were developed for homogeneous slags. Thus, a new approach for the thermodynamic modelling of the P-distribution between a heterogeneous slag and liquid iron covering the total blowing period in the converter was developed and incorporated in a kinetic de-phosphorisation model using [SimuSage](#). The two phase diagrams below show the most relevant phase relationships pertaining to the de-phosphorisation as calculated from the GTOx database:

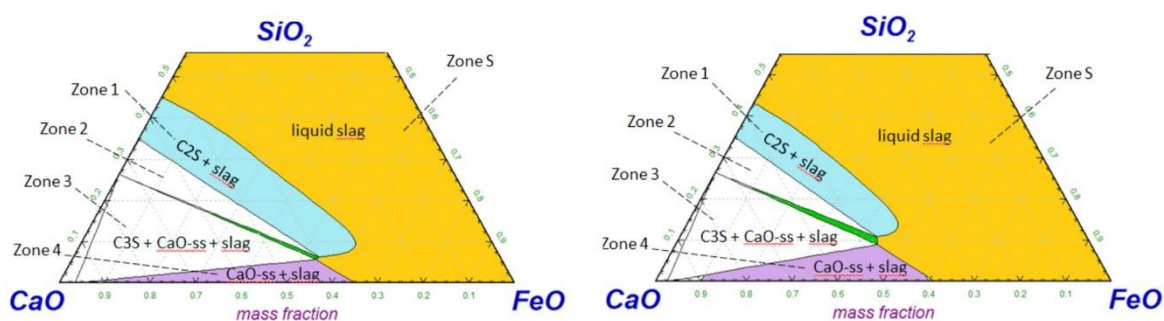


Figure 6: Liquidus isothermals of the system CaO-FeO_x-SiO₂ in equilibrium with liquid Fe at 1550 °C (left) and 1700 °C (right).

Figure 6 shows two isothermal sections of the CaO-FeO_x-SiO₂ system. Depending on processing conditions (lime addition, temperature, blow rate, stirring etc.), the actual slag composition mostly varies between the yellow (fully liquid) and light blue (liquid plus C₂S-C₃P) regions. The ranges marked in the diagram are discussed in further detail in the paper [Khadhraoui2018].

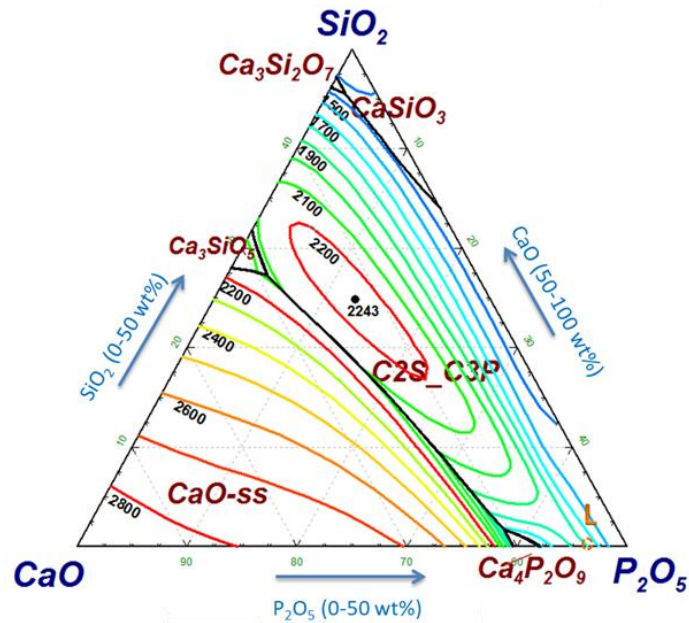


Figure 7: The CaO-rich corner of the CaO-P₂O₅-SiO₂ system. Note the primary precipitation range of the C₂S-C₃P phase.

Figure 7 shows the liquidus surface in the CaO-rich corner of the CaO-P₂O₅-SiO₂ system. It becomes obvious that the very complex pseudo-binary solution phase between the compositions 2CaO·SiO₂ and 3CaO·P₂O₅ called C₂S-C₃P is very stable with a congruent melting point at 2243 K. In the BOF process, this behavior leads to the above-mentioned heterogeneous slags, i.e. slags containing both solid and liquid phase contributions. The partitioning of phosphorous between the heterogeneous slag and the steel bath is heavily affected by the presence of the solid silicate phosphate. Using GTOx as the basis of a BOF model enables consideration of this complex interdependence.

References

[Khadhraoui2019] S. Khadhraoui, K. Hack, T. Jantzen, and H. Odenthal, Study of the State of Industrial P₂O₅-Containing Slags Relevant to Steelmaking Processes Based on a New Thermodynamic Database Developed for CaO-FeO_x-P₂O₅-SiO₂-MnO-MgO-Al₂O₃ Slags – Part I: Ternary and Lower Order Systems, steel research int. 90 (2019).

[Khadhraoui2018] S. Khadhraoui, H.-J. Odenthal, S. Das, M. Schlautmann, K. Hack, B. Glaser and R. Wolf, A new approach for modelling and control of dephosphorization in BOF converter, La Metallurgia Italiana (2018), n. 11-12, 5-16.

Refractory applications

To improve the lifetime of refractory materials, the potential corrosion by slags needs to be minimized. For this purpose, a counter-cross calculation for the refractory/slag interface is often used [Udagawa1993] [Carlborg2018]. In such a calculation two well specified end compositions are treated like two “components” of a pseudo-binary system. The overall composition of the system is given by the fraction of one of the end compositions. This fraction is changed from 0 to 1 and the resulting equilibrium phase distribution is generated (see below).

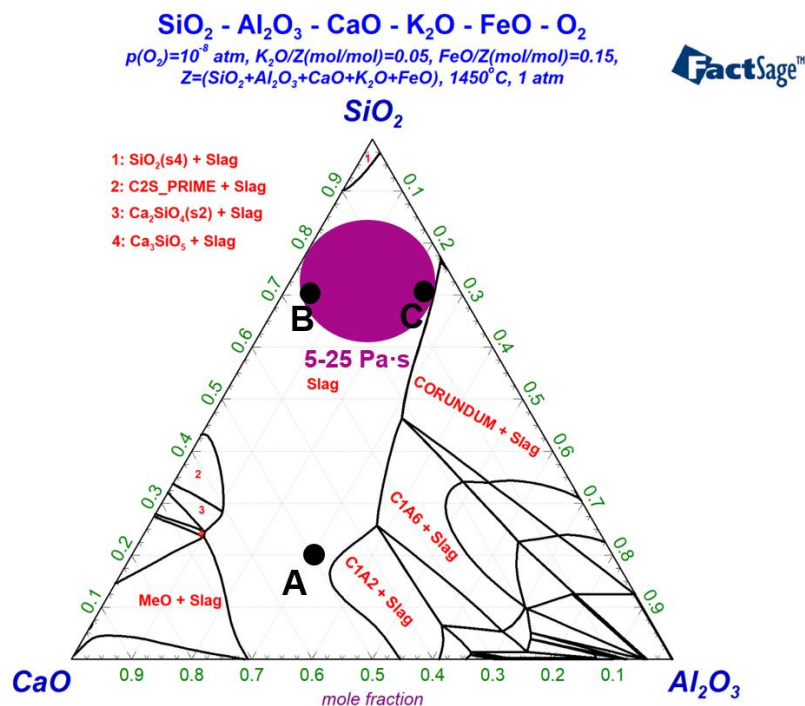


Figure 8: Phase diagram of the system SiO₂-Al₂O₃-CaO-K₂O-FeO at 1450 °C and reducing atmosphere with indicated target viscosity range of 5-25 Pa·s.

The phase diagram of a typical gasifier slag system SiO₂-Al₂O₃-CaO-K₂O-FeO at 1450 °C and under a reducing atmosphere is shown in Figure 8. As an example, a counter-cross reaction between an Al₂O₃-based refractory material (for simplicity pure alumina is used) and a slag A is illustrated in Figure 9. Although the refractory can react with the slag A, the formation of three solid solution phases, i.e. CaO·6Al₂O₃, Kaliophilite-HT, and CaO·2Al₂O₃ results in the formation of a protective layer on the surface of the refractory. It should be mentioned that in a counter-cross calculation the diffusion rate of each species in both slag and refractory phases is assumed to be the same.

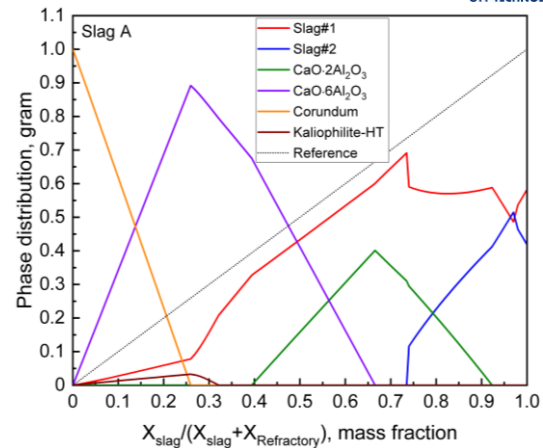


Figure 9: Potential reactions between refractory and slag using a counter-cross calculation.

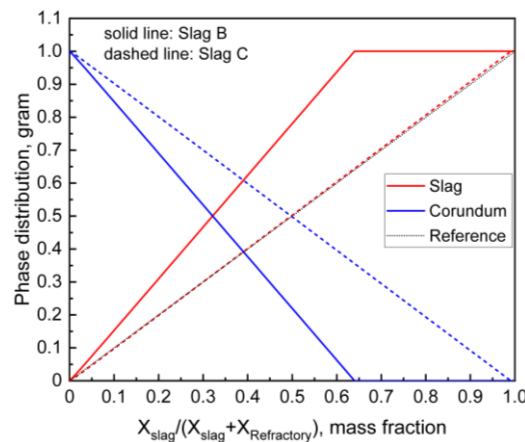


Figure 10: Comparison of the corroding effect of two slags B and C on an Al_2O_3 -based refractory material.

Under the constraint that the viscosity range for slags in entrained flow gasifiers is recommended to be in the range of 5 - 25 Pa·s, the corrosion of the two slag candidates B and C on the Al_2O_3 -based refractory material is compared, as shown in Figure 10. Compared to the dotted line as reference (i.e. without any reaction between the slag and the refractory material), an obvious increase in slag mass is noticed for the slag B, which indicates the dissolution of the refractory material into the slag. It will cause a decrease in lifetime of the refractory material. An adjustment of the slag composition from slag B to C can almost eliminate the dissolution.

References

- [Udagawa1993] E. Udagawa, E. Maeda, T. Nozaki, Slag penetration into magnesia and alumina monolithic refractories. In Unitecr'1993 Congress. Refractories for the New World Economy. Proc. Conf. Sao Paulo 31 (1993).
- [Carlborg2018] M. Carlborg, F. Weiland, C. Ma, R. Backman, I. Landälv, H. Wiinikka, Exposure of refractory materials during high-temperature gasification of a woody biomass and peat mixture, J. Eur. Ceram. Soc. 38 (2018) 777-787.

Distribution of Vanadium

Vanadium oxides were added to the GTOx database because of their important role in ferro-titanium metallurgy as well as in petroleum coke gasification. With the knowledge about the complex behavior of vanadium in slags as well as in liquid metal alloys it is possible to calculate the vanadium distribution ratios $(V)/[V]$, called L_v , between iron melts and slags in a wide range of temperatures and compositions, corroborating the validity of the model under reducing conditions. An example is shown in Figure 11.

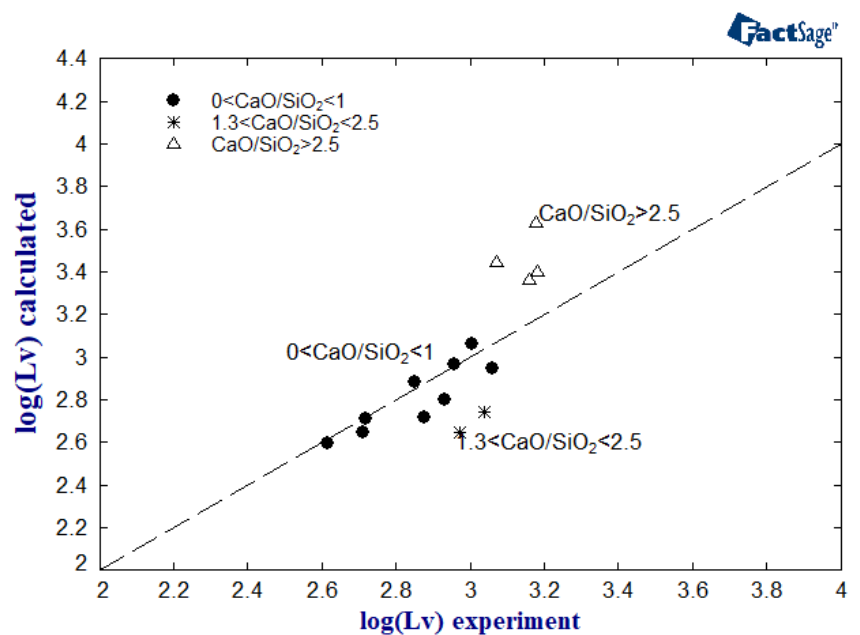


Figure 11: Relationship between the calculated and experimentally determined vanadium distribution at 1650 °C [Inoue1982].

The additionally developed viscosity model shows good agreement between the calculated and experimental values in vanadium-containing slags. More details can be found in the publication by Jantzen et al. [Jantzen2021].

References

[Inoue1982] R. Inoue, H. Suito, Distribution of Vanadium between Liquid Iron and MgO Saturated Slags of the System CaO-MgO-FeO_x-SiO₂, Trans. Iron Steel Inst. Jpn. 22 (1982) 705-714.

[Jantzen2021] T. Jantzen, E. Yazhenskikh, K. Hack, M. to Baben, G. Wu, M. Müller, Addition of V₂O₅ and V₂O₃ to the CaO-FeO-Fe₂O₃-MgO-SiO₂ database for vanadium distribution and viscosity calculation, Calphad 74 (2021) 102284.

Slag formation, fouling, and condensation from coal/biomass/waste gasification and combustion

During gasification and combustion, the majority of the inorganic species are converted to slag, whereas other inorganic species behave as fly ash entrained in the syngas or flue gas. To understand the slag formation process, ash fusion temperatures (AFTs) are often used in practice. Thermochemical calculations provide insight on AFTs of different fuel ashes with respect to temperature, composition, and atmosphere. Three ash samples from the literature were taken as examples, their compositions and flow temperatures are given in Table 1.

Sample	Composition of ashes, wt%								AFT, °C
	SiO ₂	Al ₂ O ₃	CaO	MgO	Na ₂ O	Fe ₂ O ₃	TiO ₂	SO ₃	
Ash 1	30.7	27.8	9.21	1.06	0.42	20.6	0.82	8.04	1340
Ash 2	41.5	36.5	7.12	0.56	0.18	8.32	1.33	2.67	1465
Ash 3	44.8	36.3	5.49	0.85	0.34	4.96	1.98	2.9	1520

Table 1: Composition and ash fusion temperatures (AFT) of three selected ash samples [Wang2021].

The phase distribution of Ash 1 as function of temperature significantly differs for different atmospheres, as shown in Figure 12, where the reducing atmosphere is defined as a gas mixture of 60%CO-40%CO₂ while the oxidizing atmosphere is a gas mixture of 21%O₂-79%N₂, i.e. air.

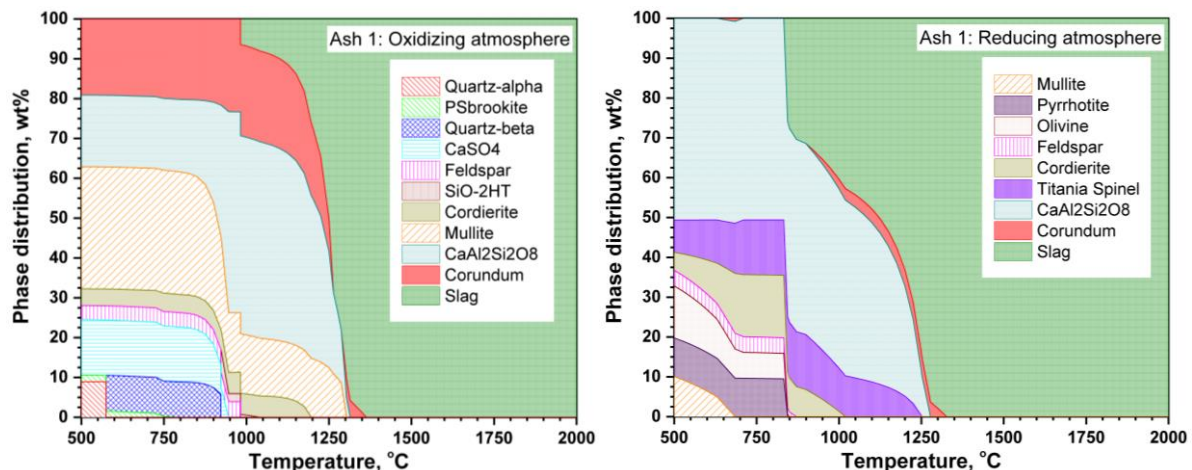


Figure 12: Phase distribution of Ash 1 at oxidizing (left) and reducing (right) atmosphere.

Figure 13 compares the mass fraction of the liquid phase for the three different ashes. It can be seen that the temperature at which the ash is fully liquid is an excellent predictor of the experimentally measured flow temperature (FT).

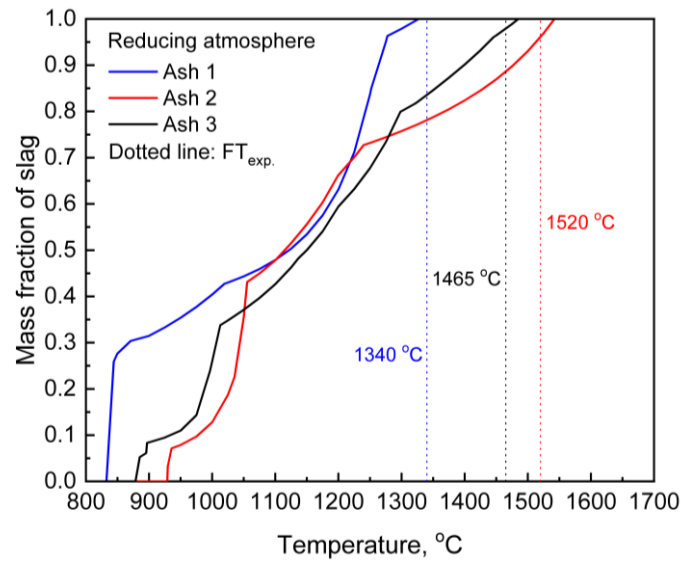


Figure 13: Relation of mass fraction of slag with experimental flow temperature (FT).

The mass fraction of a slag can also be used to evaluate the fouling behavior of fly ashes on surfaces of the downstream units of a gasifier or combustion chamber, and the description is reported elsewhere in detail [Kleinhans2018]. In addition to fly ash, trace elements released from fuels will also condense on these surfaces. The condensation mechanism of Zn vapor, taken as an example, can be illustrated using the Scheil-Gulliver cooling model [Zhao2021]. Figure 14 implies a supercooling of the condensate ZnO (a pure solid phase). The difference between the experimental and calculated ZnCl₂ condensate has been discussed in detail elsewhere [Zhao2021].

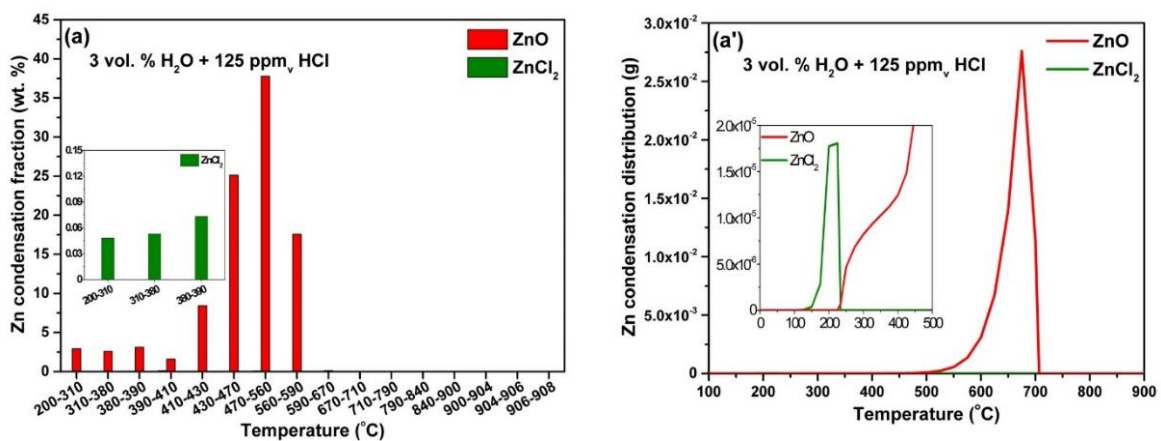


Figure 14: (a) IC and ICP-OES measurements for zinc-containing species under atmosphere containing HCl with 3 vol% steam compared to (a') the predictions with FactSage using the Scheil-Gulliver cooling model [Zhao2021] (Reprinted with permission by Elsevier).

References

[Wang2021] Hui Wang, Lihua Cheng, Jianglong Pu, Jigang Zhao, Melting Characteristics of Coal Ash and Properties of Fly Ash to Understand the Slag Formation in the Shell Gasifier, ACS Omega 24 (2021) 16066-16075.

[Kleinhans2018] Ulrich Kleinhans, Christoph Wieland, Flemming J. Frandsen, Hartmut Spliethoff, Ash formation and deposition in coal and biomass fired combustion systems: Progress and challenges in the field of ash particle sticking and rebound behavior, Progress in Energy and Combustion Science 68 (2018) 65-168.

[Zhao2021] Xin Zhao, Guixuan Wu, Jia Qi, Moritz to Baben, Michael Müller, Investigation on the condensation behavior of the trace element zinc in (Ar/H₂O/HCl/H₂S) gas mixtures and its practical implications in gasification-based processes for energy and power generation, Fuel 295 (2021) 120600.

Optimization of slag mobility in entrained flow gasifiers

In order to achieve smooth slag flow and tapping during the operation of entrained flow slagging gasifiers, a viscosity range $\ln(\eta, \text{Pa}\cdot\text{s})$ of 1.6–3.2 at 1400–1550 °C is desirable. Typically, blended feedstocks with the addition of fluxing agents are used to adjust the slag viscosity. As shown in Figure 15(a), the viscosity of the model gasifier slags (for the composition see Table 2), taken as examples, is outside of the desirable viscosity range.

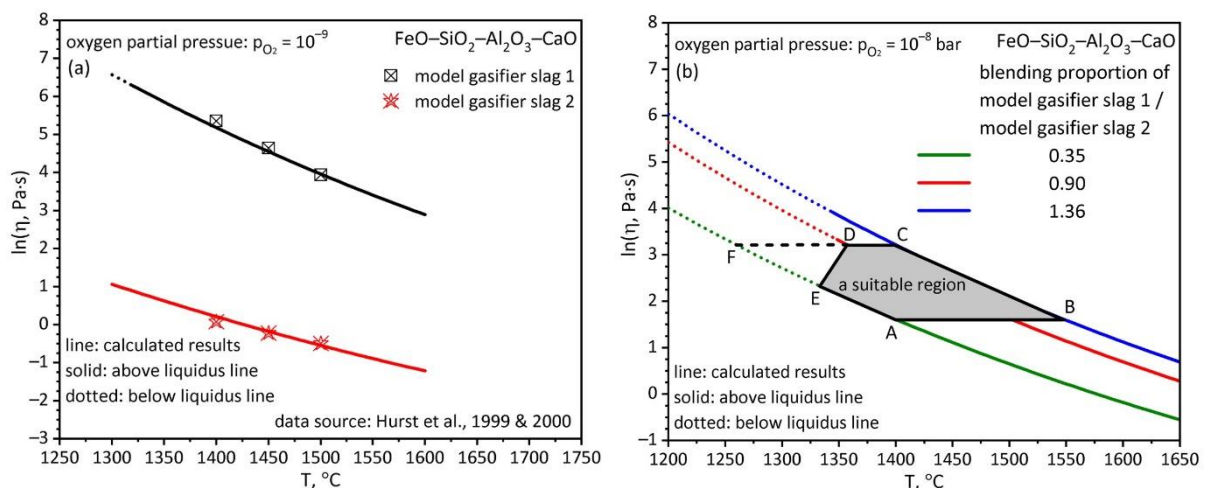


Figure 15: (a) Viscosity predictions compared to the experimental data [Hurst1999] [Hurst2000] of model gasifier slags at an oxygen partial pressure of 10^{-9} bar, (b) Selection of a suitable blending proportion of slags [Wu2021] (Reprinted with permission by Elsevier).

Model gasifier slag	Composition, mol%				$T_{\text{liquidus}}, ^\circ\text{C}$
	SiO ₂	Al ₂ O ₃	CaO	FeO	
1	68.61	13.84	12.59	4.96	1318
2	42.55	11.42	33.18	12.86	1245

Table 2: Composition of the model gasifier slags in Figure 15 [Wu2019] (Reprinted with permission by Elsevier).

Figure 15(b) demonstrates desirable blending proportions of the selected slags as determined by the present viscosity model, where the oxygen partial pressure is assumed to be 10^{-8} bar, corresponding to a typical value during the operation of an entrained flow slagging gasifier. As a result, the gray area ABCDE in the figure indicates a suitable region of blending selected slags in combination with the liquidus information, i.e. the point E refers to a melting temperature of 1333 °C. It can be seen that the operating temperature can vary from 1333 °C to 1548 °C, and the blending proportion can vary from 0.35 to 1.36, where the blending proportion of 0.9 should result in an optimum viscosity of 15 Pa·s (i.e. $\ln(\eta, \text{Pa}\cdot\text{s})$ of 2.7) at 1400 °C. Information regarding fluctuations of the operating temperature, slag composition, and atmosphere

can be used to further determine an optimum blending proportion. For the determination of blending proportions of three or more slags, please see [Wu2019].

References

[Wu2019] Guixuan Wu, Sören Seebold, Elena Yazhenskikh, Joanne Tanner, Klaus Hack, Michael Müller, Slag mobility in entrained flow gasifiers optimized using a new reliable viscosity model of iron oxide containing multicomponent melts, *Applied Energy* 236 (2019) 837–849.

[Hurst1999] H.J. Hurst, F. Novak, J.H. Patterson, Viscosity measurements and empirical predictions for some model gasifier slags, *Fuel* 78 (1999) 439-444.

[Hurst2000] H.J Hurst, J.H Patterson, A Quintanar, Viscosity measurements and empirical predictions for some model gasifier slags-II, *Fuel* 79 (2000) 1797-1799.

Assessment examples

In this section, a selected number of cases for characteristic thermodynamic assessments which form part of the GTOx database is presented.

ZnO-P₂O₅

Available experimental data was used for the generation of thermodynamic data for the system ZnO-P₂O₅. The model of non-ideal associated solutions was used to describe the liquid phase containing the following associates: ZnO·P₂O₅, 2ZnO·P₂O₅ and 3ZnO·P₂O₅. Seven literature sources concerning phase equilibria and five references dealing with the internal structure of the liquid phase have been used to generate a consistent thermodynamic dataset for the system. Figure 16 shows the phase diagram and Figure 17 the phase-internal species distribution in the liquid phase as function of the mole fraction of ZnO calculated with the Gibbs energy dataset. Calculated associate species distribution in the liquid phase ZnO-P₂O₅ at 1000 °C is compared with available experimental data (NMR, EMF, Raman). The calculation is done for the middle temperature of the experimental ones which cover 900 °C, 1000 °C and 1100 °C. The calculated results show a very good representation for all temperatures. Also the agreement between experimental and calculated phase boundaries in Figure 16 is very good.

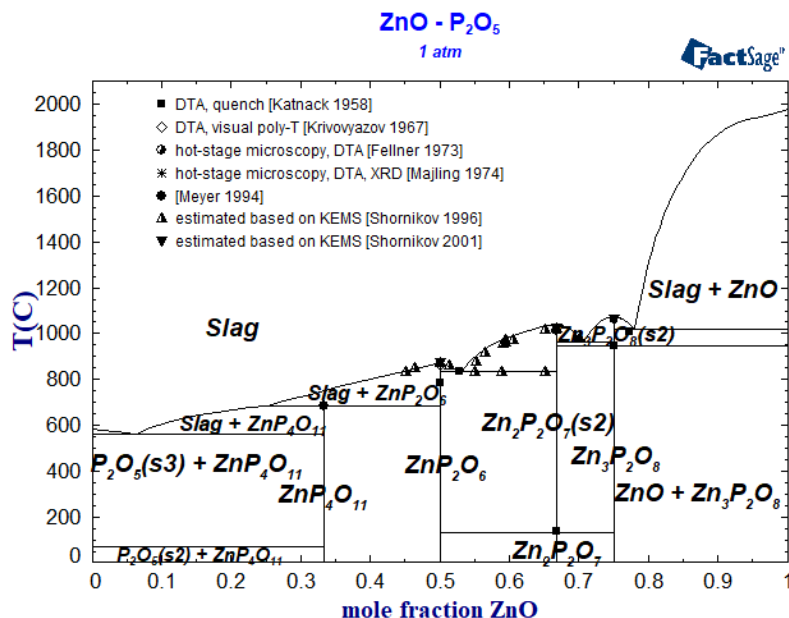


Figure 16: Calculated phase diagram of the system P₂O₅-ZnO compared with experimental data.

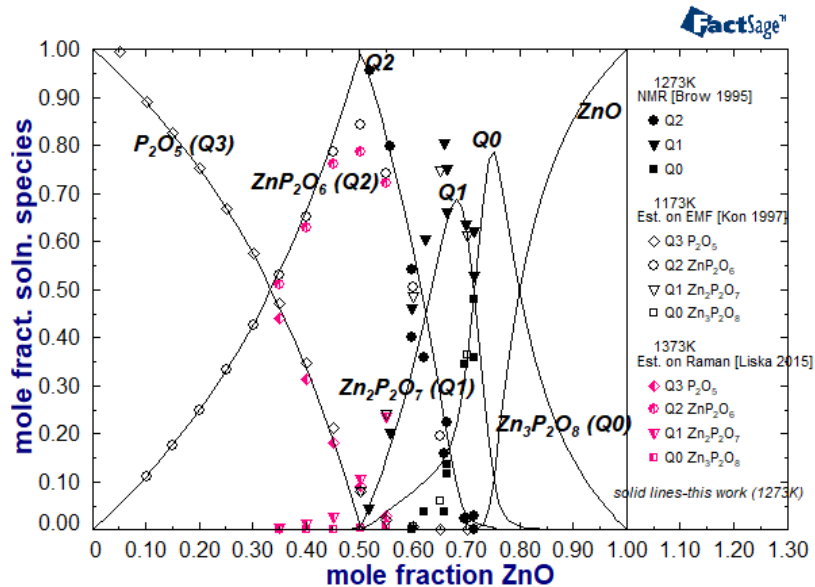


Figure 17: Calculated associate species distribution in the liquid phase P_2O_5 -ZnO at 1000 °C compared with experimental data (NMR, Raman).

The experimentally observed structural units are considered as liquid constituents in the framework of the modified non-ideal associate species model. This fact indicates that the modified non-ideal associate species model is appropriate for the prediction of the structural features in the liquid phase with a direct link to, for example, the viscosity of the melt published by Wu et al. [Wu2019].

References

- [Katnack1958] F.L. Katnack, F.A. Hummel, Phase Equilibria in the System ZnO- P_2O_5 , J. Electrochem. Soc. 105 (3) (1958) 125-133.
- [Shornikov1996] S.I. Shornikov, A.L. Shilov, M.M. Shultz, A mass spectrometric study of the thermodynamic properties of melts in the ZnO- P_2O_5 system, Zh. Phys. Khim. 70 (3) (1996) 485-491.
- [Krivovyazov1967] E.L. Krivovyazov, K.K. Palkina, N.K. Voskresenskaya, Diagrammi plavkosti dvojnih sistem iz metafosfata zinka i metafosfatov Na ili K (in Engl. Melting diagram of the binary systems $Zn(PO_3)_2$ -(Na or K) PO_3), Dokl. Akad. Nauk SSSR, Chemistry 174 (3) (1967) 610-613.
- [Fellner1973] P. Fellner, J. Majling, Calculation of liquidus curves in phase diagrams $Na_4P_2O_7$ - $Mg_2P_2O_7$ and $Na_4P_2O_7$ - $Zn_2P_2O_7$, Chem. zvesti 27 (6) (1973) 728-731.
- [Majling1974] J. Majling, S. Palco, F. Hanic, J. Petrovic, Phase equilibria in the system $Na_4P_2O_7$ - $Zn_2P_2O_7$, Chem. zvesti 28 (3) (1974) 294-297.
- [Meyer1994] K. Meyer, H. Hobert, A. Barz, D. Stachel, Infrared spectra and structure of various crystalline ultraphosphates and their glasses, Vibrational Spectroscopy 6 (3) (1994) 323-332.

[Shornikov2001] S.I. Shornikov, Vaporization processes and thermodynamic properties of zinc phosphates, Proc. Electrochemical Society 12 (2001) 316-321.

[SGPS] SGPS - SGTE Pure Substances database (v13.1) 2017.

[Konakov1997] V.G. Konakov, B.A. Shakhmatkin, M.M. Shultz, Thermodynamic properties of $\{x\text{ZnO}+(1-x)\text{P}_2\text{O}_5\}(\text{l})$, J. Chem. Thermodynamics 29 (7) (1997) 785-795.

[Brow1995] R.K. Brow, D.R. Tallant, S.T. Myers, C.C. Phifer, The short-range structure of zinc polyphosphate glass, J. Non-Crystalline Solids 191 (1995) 45-55.

[Liška2015] M. Liška, M. Lissová, A. Plško, M. Chromčíková, T. Gavenda, J. Macháček, Thermodynamic model and Raman spectra of ZnO–P₂O₅ glasses, J. Therm. Anal. Calorim. 121 (1) (2015) 85-91.

[Wu2019] G. Wu, S. Seebold, E. Yazhenskikh, J. Tanner, K. Hack, M. Müller, Slag mobility in entrained flow gasifiers optimized using a new reliable viscosity model of iron oxide-containing multicomponent melts, Applied Energy, 236 (2019) 837-849.

CaO-ZnO-P₂O₅

The following ternary phases are included in the present database along with the Slag phase: the solid solutions based on Ca₃P₂O₈ (C3P-C2S, HT; C3P-alpha, MT; C3P-beta, LT) and on Zn₃P₂O₈ (Z3P-beta, HT; Z3P- alpha, LT) as well as the intermediate solid solution based on CaZn₂P₂O₈-HT (CZ2P-HT) according to [Kreidler1967, Carbajal2011]. The phase boundaries reported in these two sources have been used to optimize the parameters of the liquid phase as well as the various solid phases. The resulting phase diagrams are shown in Figure 18 and Figure 19. It should be noted in particular that the system has been considered as fully water-free. Thus, the phase Ca₄P₂O₉ appears in the diagrams instead of HAp (HAp=hydroxyapatite Ca₁₀(PO₄)₆(OH)₂), which is observed experimentally due to water impurities.

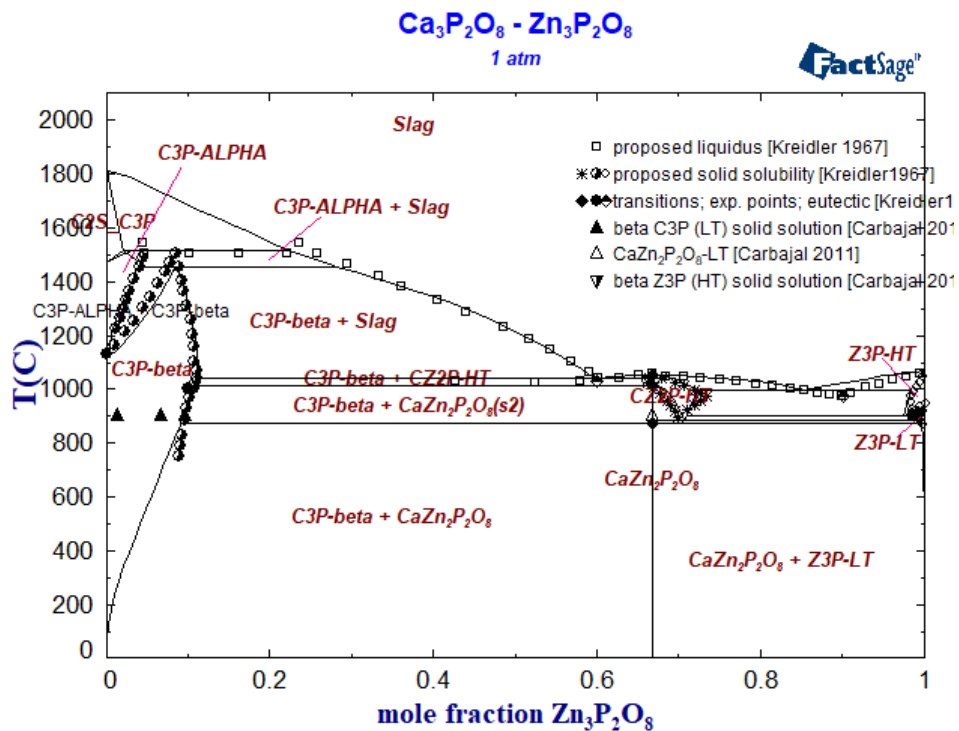


Figure 18: Calculated phase diagram of the system Ca₃P₂O₈-Zn₃P₂O₈ compared with experimental data [Kreidler1967, Carbajal2011].

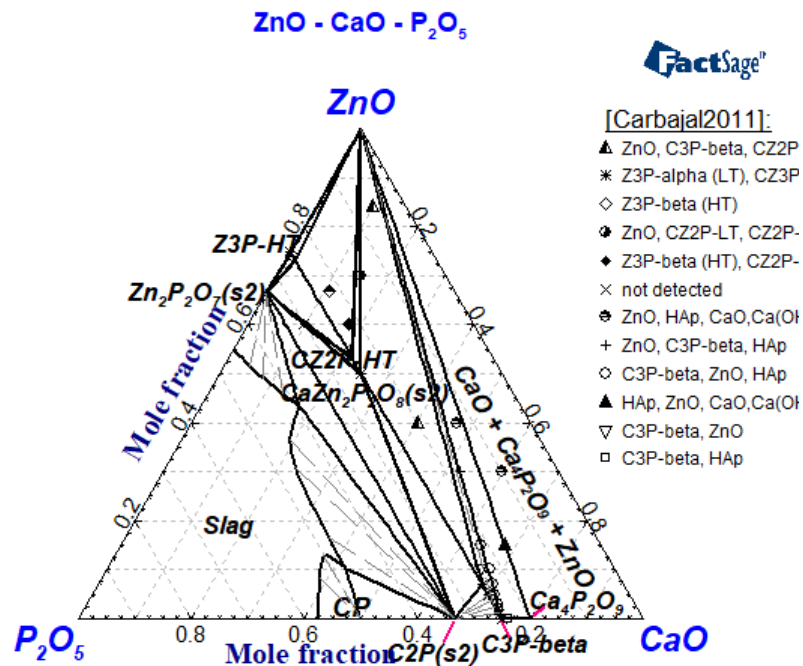


Figure 19: Calculated isothermal section at 900 °C in the ternary system CaO-P₂O₅-ZnO compared with experimental data [Carbajal2011].

References

[Kreidler1967] E.R. Kreidler, F.A. Hummel, Phase equilibriums in the System Ca₃(PO₄)₂-Zn₃(PO₄)₂, Inorg. Chem. 6 (3) (1967) 524-528.

[Carbajal2011] L. Carbajal, M.A. Sainz, S. Serena, A.C. Caballero, Á. Caballero, Solid-State Compatibility in Two Regions of the System ZnO-CaO-P₂O₅, Journal of the American Ceramic Society 94 (7) (2011) 2213-2219.

Al₂O₃-Li₂O-MgO

MgAl₂O₄ and LiAl₅O₈ (or Li_{0.5}Al_{0.5}Al₂O₄) form a complete spinel solid solution in the Li₂O-MgO-Al₂O₃ system [Menzheres1978, Izquierdo1980]. Spinel is an oxide of the general type A^TB^O₂O₄ which has a very compact oxygen structure, with cations in tetrahedral (T) and octahedral (O) oxygen coordination. Simple examples are MeO·Me₂O₃ which can be described with the formula (Me²⁺)(Me³⁺)₂(O²⁻)₄, where the divalent cations occupy the tetrahedral and the trivalent cations the octahedral sublattice sites. This makes it more obvious that the valence state of the metals plays an important part for the existence of this phase. MgAl₂O₄ has a normal spinel structure where Mg²⁺ is mostly placed on tetrahedral sites and Al³⁺ occupies octahedral sites. In the opposite system, Li_{0.5}Al_{2.5}O₄ has an inverse spinel structure where Al³⁺ combined with Li¹⁺ are located on the octahedral sublattice, and Al³⁺ occupies the tetrahedral sublattice. Using a combined cationic species on the tetrahedral sublattice (Li_{0.5}Al_{0.5}²⁺) deals with the charge compensation between the monovalent and the trivalent ion. The isothermal section for 1400 °C in the Al₂O₃-Li₂O-MgO system is presented in Figure 20 where MgAl₂O₄ and LiAl₅O₈ form a complete solid solution.

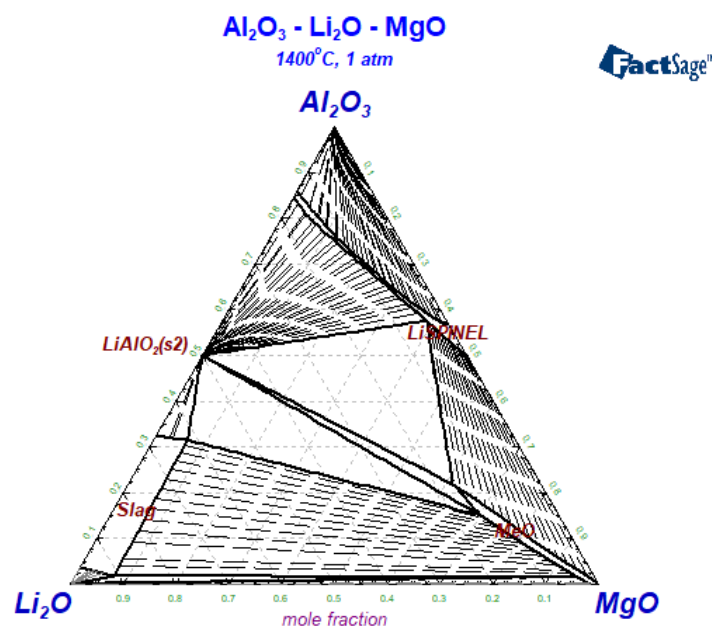


Figure 20: Isothermal section at 1400 °C in the Al₂O₃-Li₂O-MgO system.

References

[Menzheres1978] L. T. Menzheres, N. P. Kotsupalo, A. S. Berger, Zh. Neorg. Khim., 23 [10] 2804-2809 (1978).

[Izquierdo1980] G. Izquierdo, A. R. West, J. Am. Ceram. Soc., 63 [3-4] 227-227 (1980).

Viscosity modelling

Model parameters for the viscosity of oxide melts have been assessed, where available, by using the experimental data for pure oxides and selected binary and ternary systems. Great care has been taken in order to cover the well-known experimental facts by the modelling. These are: the lubricant effect, the weak lubricant effect, and the charge compensation effect. The following series of diagrams (Figure 21) shows the successful use of the model for all these characteristic features.

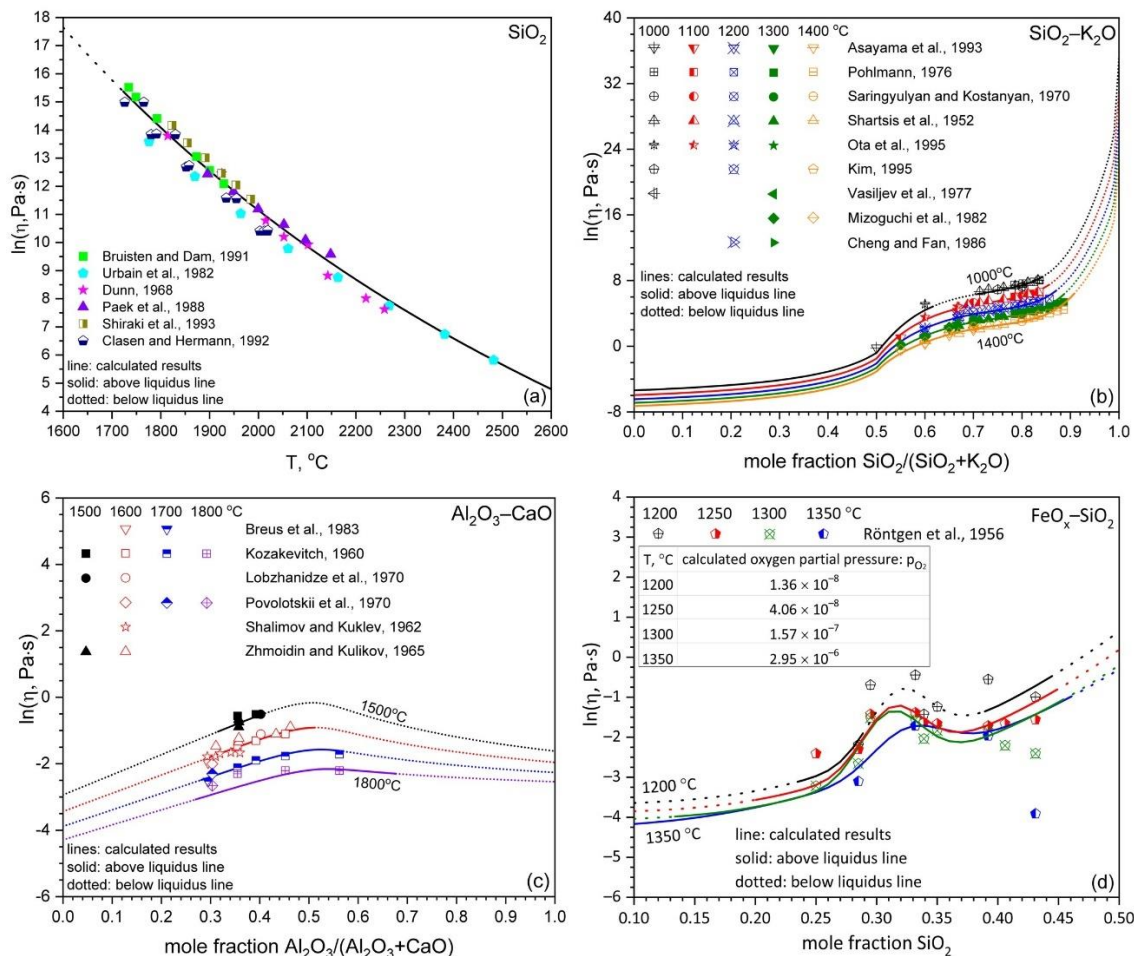


Figure 21: Comparison between experimental data and calculated data for the selected oxide melts SiO_2 (a), $\text{SiO}_2\text{-K}_2\text{O}$ (b), $\text{Al}_2\text{O}_3\text{-CaO}$ (c), and $\text{FeO}_x\text{-SiO}_2$ (d) [Wu2015,Part1] [Wu2018] (Reprint with permission by Elsevier).

For molten silica, the viscosity of more than 5 MPa·s ($\ln(\eta, \text{Pa}\cdot\text{s}) \approx 15.5$) approaching the melting temperature is well reproduced by the present model, as shown in Figure 21(a). It is seen from Figure 21(b) that the viscosity decreases drastically when a small amount of a network modifier, here K_2O , is added into the pure silica melt, where the network modifier plays the role of a lubricant allowing silica clusters to glide more easily alongside each other ("*lubricant effect*"). Another clearly

noticeable but less strong decrease of the viscosity occurs around the SiO_2 content of 0.55 mole fraction (“*weak lubricant effect*”) due to possible ring structures. The present model can very well describe both these effects.

The present model also reproduces the viscosity maximum due to the “*charge compensation*” of Al_2O_3 with CaO , as shown in Figure 21(c). The influence of the oxygen partial pressure on the viscosity behavior of systems containing multivalent iron oxide has also been considered. It is seen from Figure 21 (d) that a local viscosity maximum around the fayalite composition occurring in the binary system FeO-SiO_2 is described by the present model, where the position of the local viscosity maximum and its order of magnitude vary with temperature and oxygen partial pressure.

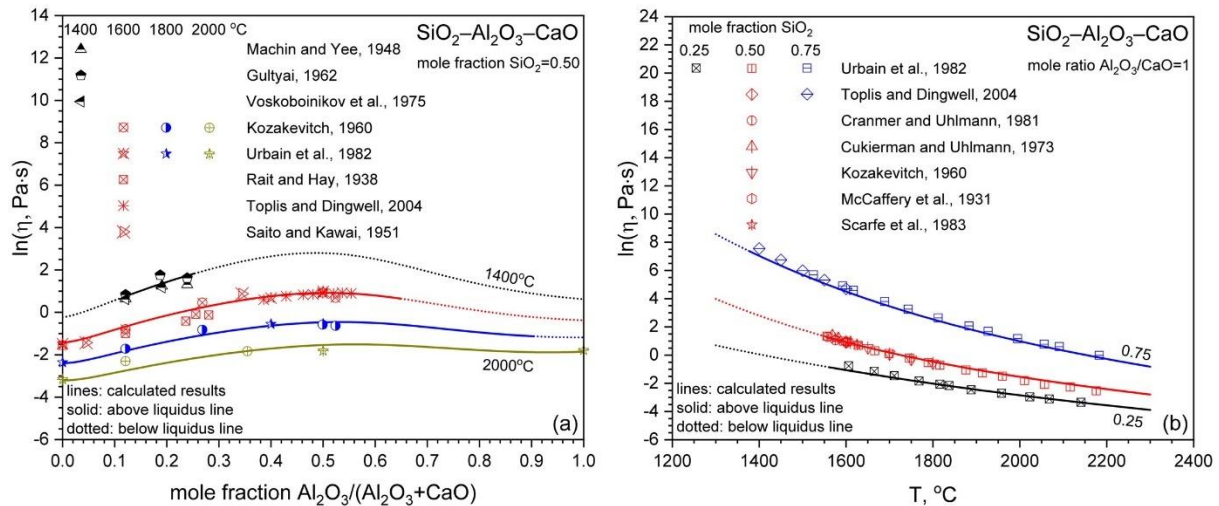


Figure 22: Comparison between experimental data and calculated data for the system $\text{SiO}_2\text{-Al}_2\text{O}_3\text{-CaO}$ [Wu2015,Part2] (Reprinted with permission by Elsevier).

The extension of the model from low-order systems to high-order systems has been evaluated, as reported in detail elsewhere [Wu2015,Part2] [Wu2019] [Hack2019]. Figure 22 shows an example regarding the viscosity behavior induced by the charge compensation effect in the ternary system $\text{SiO}_2\text{-Al}_2\text{O}_3\text{-CaO}$. As shown in Figure 22(a), the viscosity maximum is well described by the present model around the fully charge-compensated composition, which is CaAl_2O_4 . The present model reproduces the order of magnitude of the viscosity maximum with increasing SiO_2 content. At the fully charge-compensated composition, the trend of the viscosity with temperature, as shown in Figure 22(b), has also been well predicted. This indicates a good quality regarding the assessment of model parameters.

It is worth noting that the values of the model parameters are not just fitting parameters determined by minimization of the difference between experimental data and model calculations. They have a clear-cut physical meaning, i.e. for each structural unit they represent the activation energy for viscous flow which increases as the ability of network formation rises. In addition, viscosities extrapolated to regions where no experimental data are available in literature have also been checked for reasonable behavior.

References

[Wu2015,Part1] Guixuan Wu, Elena Yazhenskikh, Klaus Hack, Erwin Wosch, Michael Müller, Viscosity Model for Oxide Melts Relevant to Fuel Slags. Part 1: Pure Oxides and Binary Systems in the System $\text{SiO}_2\text{--Al}_2\text{O}_3\text{--CaO--MgO--Na}_2\text{O--K}_2\text{O}$, Fuel Processing Technology 137 (2015) 93–103.

[Wu2018] Guixuan Wu, Sören Seebold, Elena Yazhenskikh, Klaus Hack, Michael Müller, Viscosity Model for Oxide Melts Relevant to Fuel Slags. Part 3: The Iron Oxide Containing Low Order Systems in The System $\text{SiO}_2\text{--Al}_2\text{O}_3\text{--CaO--MgO--Na}_2\text{O--K}_2\text{O--FeO--Fe}_2\text{O}_3$, Fuel Processing Technology 171 (2018) 339–349.

[Wu2015,Part2] Guixuan Wu, Elena Yazhenskikh, Klaus Hack, Michael Müller, Viscosity Model for Oxide Melts Relevant to Fuel Slags. Part 2: The System $\text{SiO}_2\text{--Al}_2\text{O}_3\text{--CaO--MgO--Na}_2\text{O--K}_2\text{O}$, Fuel Processing Technology 138 (2015) 520–533.

[Wu2019] Guixuan Wu, Sören Seebold, Elena Yazhenskikh, Joanne Tanner, Klaus Hack, Michael Müller, Slag mobility in entrained flow gasifiers optimized using a new reliable viscosity model of iron oxide containing multicomponent melts, Applied Energy 236 (2019) 837–849.

[Hack2019] Klaus Hack, Guixuan Wu, Elena Yazhenskikh, Tatjana Jantzen, Michael Müller, A CALPHAD approach to modelling of slag viscosities, Calphad 65 (2019) 101–110.

Density modelling

The model parameters have been assessed using the existing experimental data for pure oxides as well as binary and ternary subsystems. Due to a limited availability of experimental density data for pure oxides, the calculated densities by Ghiorso and Kress [Ghiorso2004] are used to derive the model parameters regarding the partial molar volume and partial molar thermal expansion.

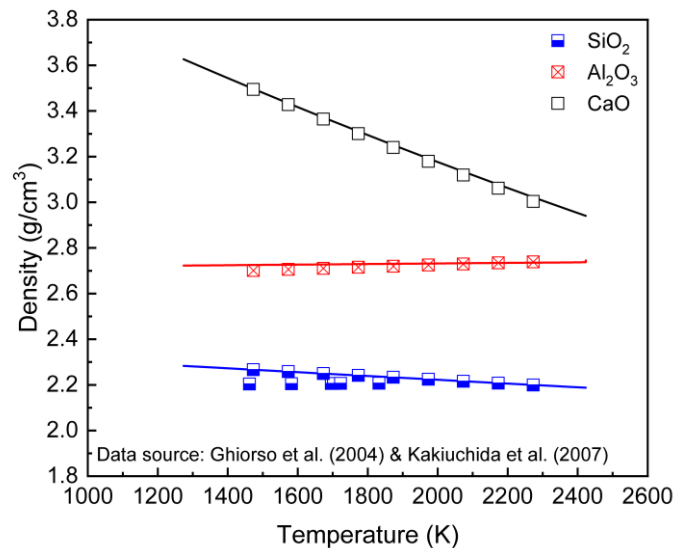


Figure 23: Comparison between the existing data [Ghiorso2004] [Kakiuchida2007] and model predictions for SiO₂, Al₂O₃ and CaO.

As shown in Figure 23, for SiO₂ and CaO the density usually decreases as temperature increases. However, the figure also shows that the density of Al₂O₃ increases slightly with increasing temperature. This unusual effect may be caused by the structural evolution of OAl₃ triclusters. As temperature increases, the stability of these triclusters decreases and the oxygen coordination number increases, which leads to a decrease in the molar volume of Al₂O₃. This structural variation with respect to the temperature requires a negative partial molar thermal expansivity of Al₂O₃.

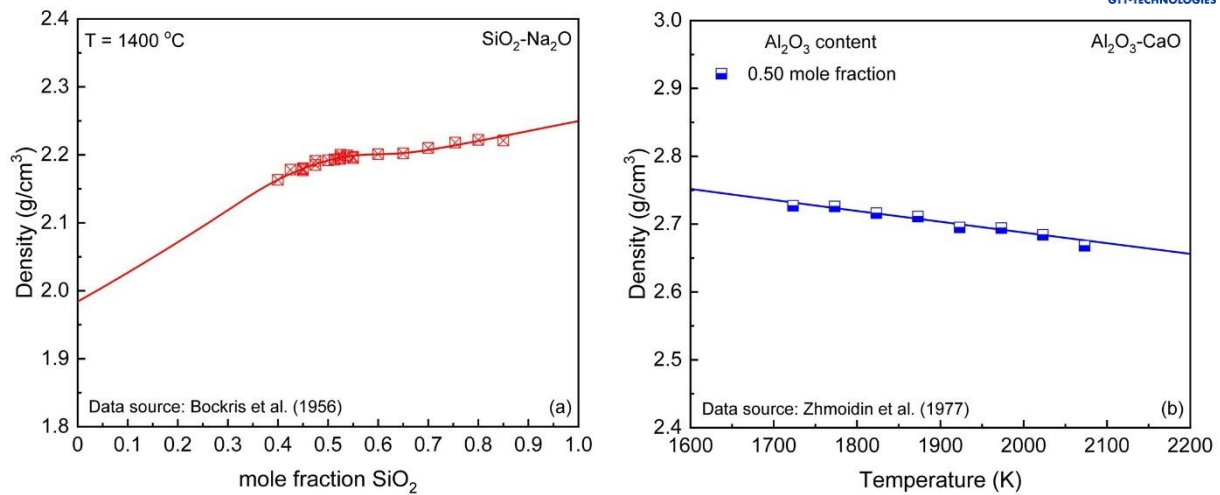


Figure 24: Comparison between the existing data [Bockris1956] [Zhmoidin1977] and model predictions for the binary systems SiO₂-Na₂O (a) and Al₂O₃-CaO (b).

The experimental data of the binary system SiO₂-Na₂O are well reproduced by the present model, as shown in Figure 24(a), where a small hump in density occurs probably due to the formation of a ring structure. Figure 24(b) shows that the model predictions are in good agreement with the experimental data of the binary system Al₂O₃-CaO. It is seen that the density decreases with increasing temperature, where Al₂O₃ plays a different structural role compared to that in a pure Al₂O₃ melt, because Al₂O₃ is almost fully compensated by CaO, and the quasi-tetrahedron CaAl₂O₄, rather than the OAl₃ tricluster, is dominant.

When the model is extended to the ternary system SiO₂-Al₂O₃-CaO, the model predictions are consistent with the experimental density data, as shown in Figure 25. This indicates that the structural dependence of density has been well described by the present model regarding the Al₂O₃-induced charge compensation effect.

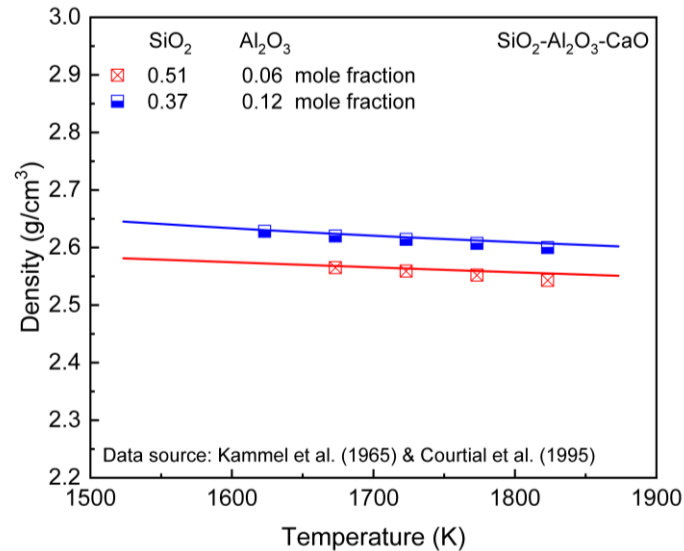


Figure 25: Comparison between the existing data [Kammel1965] [Courtial1995] and model predictions for the ternary system SiO₂-Al₂O₃-CaO.

References

- [Ghiorso2004] M. Ghiorso, V.C. Kress, An equation of state for silicate melts. II. Calibration of volumetric properties at 10⁵ Pa, *Am. J. Sci.* 304 (2004) 679-751.
- [Kakiuchida2007] H. Kakiuchida, E.H. Sekiya, N. Shimodaira, K. Saito, A.J. Ikushima, Refractive index and density changes in silica glass by halogen doping, *J. Non-Cryst. Solids* 353 (2007) 568-572.
- [Bockris1956] J. O'M. Bockris, J.W. Tomlinson, J.L. White, The structure of the liquid silicates: partial molar volumes and expansivities, *Trans. Faraday Soc.* 52 (1956) 299-310.
- [Zhmoidin1977] G.I. Zhmoidin, G.S. Smirnov, V.N. Gladkii, Effect of atmospheric composition on the density of melts of the system CaO-Al₂O₃ (in Russian), *Neorg. Mater.* 13 (1977) 552-553.
- [Kammel1965] R. Kammel, H. Winterhager, Struktur und Eigenschaften von Schlacken der Metallhüttenprozesse. V. Dichtebestimmungen und elektrische Leitfähigkeitsmessungen an Schmelzen des Systems Kalk-Tonerde-Kieselsäure, *Erzmetall.* 18 (1965) 9-17.
- [Courtial1995] P. Courtial, D.B. Dingwell, Nonlinear composition dependence of molar volume of melts in the CaO-Al₂O₃-SiO₂ system, *Geochim. Cosmochim. Acta* 59 (1995) 3685-3695.

Database compatibility

GTOx version 17 can be used alone or together with many other databases available in FactSage:

- SGPS (complex gas phases or first-order approximation for any other substance)
- FactPS (complex gas phases or first-order approximation for any other substance) (slightly lower compatibility)
- aiMP / aiOQ (zeroth-order approximation for any other substances, lower compatibility but much larger material system covered)
- FSstel (steels, several superalloys)
- SpMCBN (non-oxide ceramics and refractory alloys)
- FTlite (light metals)
- FSscopp (copper alloys)
- FSlead (lead alloys)
- SGTE solutions (general metal alloys, but data coverage for specific alloys is lower compared to the specialized databases indicated above)

NOTE: In all combinations involving one of FSstel, SpMCBN, FTlite, FSscopp, FSlead or SGTE Solutions, metallic solutions should not be selected from GTOx.

We will be happy to assist you in the selection of databases, please [contact us](#) if you have any questions!

Phases

Solid solution phases

The GTOx database contains **153 solid solution phases**. The complete list including a short description for each phase can be found in the appendix.

Solid stoichiometric compounds

The GTOx database includes **821 stoichiometric compounds**. The complete list can be found in the appendix.

Liquid slag

The Slag phase, which exhibits short range ordering as well as ranges of immiscibility, is modelled using the non-ideal modified associate model according to Spear and Besmann [Besmann2002]. The model was successfully applied for many types of systems with strong interactions [Hack2012, Yazhenskikh2014, Jantzen2016]. Moreover, this model can give a reliable phase-internal distribution of associate species, which is consistent with experimentally determined Q_n species distributions [Wu2018]. This in turn is the basis for the viscosity model discussed above. The Slag phase contains data for the following components:

Al₂O₃-CaO-CaF₂-Cr₂O₃-CuO-Cu₂O-FeO-Fe₂O₃-Li₂O-MgO-MnO-Mn₂O₃-K₂O-Na₂O-NiO-P₂O₅-SO₃-SiO₂-SrO-TiO₂-Ti₂O₃-V₂O₃-V₂O₅-ZnO

Liquid sulphate

The Liquid sulphate phase, modelled as a non-ideal associate solution, contains sulphates, sulphides, carbonates and chromates of the alkali components Na and K as well as the alkaline earth components Ca and Mg:

CaCO₃-CaS-CaSO₄-K₂CO₃-K₂CrO₄-K₂S-K₂SO₄-MgS-MgSO₄-Na₂CO₃-Na₂CrO₄-Na₂S-Na₂SO₄

Liquid metal

The Liquid-Me phase is described using a simple substitutional solution approach based on the Redlich-Kister-Muggianu polynomial expression. The liquid metal phase can be used for pure metals as well as

- liquid iron with dissolved Al, C, Ca, Cr, Cu, K, Mg, Mn, O, P, S, Si, Sr, V, Zn
- liquid Cu with dissolved Ca, Cr, Fe, Mn, Si
- liquid V with dissolved Al, Ca, C, Fe, Si, Ti
- liquid Ti with dissolved Al, V

Additionally, the Me-S systems with associate species with formula MeS (Me=Ca, Cr, Fe, Mg, Mn) are considered as liquid solution constituents in the present database [Jantzen2017, Jantzen2017-2].

References

- [Hack2012] Hack K., Jantzen T., Müller M., Yazhenskikh E., Wu G. A novel thermodynamic database for slag systems and refractory materials // Proceedings of the 5th Int. Congress on the Science and Technology of Steelmaking. ICS (2012). Dresden. Germany.
- [Yazhenskikh2014] Yazhenskikh E., Jantzen T., Hack K., Müller M. Critical thermodynamic evaluation of oxide system relevant to fuel ashes and slags: Potassium oxidemagnesium oxidesilica, *Calphad* 47 (2014), 35–49
- [Jantzen2016] Jantzen T., Hack K., Yazhenskikh E., Müller M. Evaluation of thermodynamic data and phase equilibria in the system Ca–Cr–Cu–Fe–Mg–Mn–S: Part I: Binary and quasibinary subsystems, *Calphad* 56 (2016), 270–285; Part II: Ternary and quasiternary subsystems, *Calphad* 56 (2017), 286–302.
- [Besmann2002] Besmann T.M., Spear K.E. Thermodynamic modelling of oxide glasses, *J. Am. Ceram. Soc.* 85 (2002), 2887–2894.
- [Wu2018] Wu G., Seebold S., Yazhenskikh E., Hack K., Müller M. Viscosity model for oxide melts relevant to fuel slags. Part 3: The iron oxide containing low order systems in the system $\text{SiO}_2\text{--Al}_2\text{O}_3\text{--CaO--MgO--Na}_2\text{O--K}_2\text{O--FeO--Fe}_2\text{O}_3$, *Fuel Processing Technology* 171 (2018), 339–349.
- [Jantzen2017] T. Jantzen, K. Hack, E. Yazhenskikh, M. Müller, Evaluation of thermodynamic data and phase equilibria in the system Ca–Cr–Cu–Fe–Mg–Mn–S part I: Binary and quasi-binary subsystems, *Calphad* 56 (2017) 270-285.
- [Jantzen2017-2] T. Jantzen, K. Hack, E. Yazhenskikh, M. Müller, Evaluation of thermodynamic data and phase equilibria in the system Ca-Cr-Cu-Fe-Mg-Mn-S Part II: Ternary and quasi-ternary subsystems, *Calphad* 56 (2017) 286-302.

What is new in version 17?

The current update is important for several reasons:

- Addition of Cu-O to describe secondary metallurgical processes
- Re-assessment of the $\text{Al}_2\text{O}_3\text{-SiO}_2$ system and all related higher-order systems
- Addition and improvement of sulfate and chromate systems including NiO to model hot corrosion

A list of all new and reassessed systems is provided below:

Binary systems

new		reassessed
$\text{Al}_2\text{O}_3\text{-Cu}_2\text{O}$	$\text{CuO-Na}_2\text{O}$	$\text{Li}_2\text{O-SrO}$
$\text{Al}_2\text{O}_3\text{-CuO}$	CuO-NiO	$\text{MgSO}_4\text{-NiSO}_4$
$\text{CaCO}_3\text{-K}_2\text{CO}_3$	$\text{CuO-P}_2\text{O}_5$	$\text{Na}_2\text{CO}_3\text{-Na}_2\text{SO}_4$
$\text{CaCO}_3\text{-Na}_2\text{CO}_3$	CuO-SiO_2	$\text{Na}_2\text{CrO}_4\text{-Na}_2\text{SO}_4$
$\text{CaO-Cu}_2\text{O}$	CuO-SrO	$\text{Na}_2\text{O-SrO}$
CaO-CuO	CuO-TiO_2	$\text{Na}_2\text{S-Na}_2\text{CO}_3$
$\text{Cu}_2\text{O-Li}_2\text{O}$	$\text{CuO-V}_2\text{O}_5$	
$\text{Cu}_2\text{O-MgO}$	CuO-ZnO	
$\text{Cu}_2\text{O-MnO}$	$\text{Fe}_2\text{O}_3\text{-CuO}$	
$\text{Cu}_2\text{O-Na}_2\text{O}$	$\text{FeO-Cu}_2\text{O}$	
$\text{Cu}_2\text{O-NiO}$	$\text{K}_2\text{CO}_3\text{-K}_2\text{SO}_4$	
$\text{Cu}_2\text{O-SiO}_2$	$\text{K}_2\text{CO}_3\text{-Na}_2\text{CO}_3$	
$\text{Cu}_2\text{O-SrO}$	$\text{K}_2\text{CrO}_4\text{-K}_2\text{SO}_4$	
$\text{Cu}_2\text{O-ZnO}$	$\text{K}_2\text{CrO}_4\text{-Na}_2\text{CrO}_4$	
Cu-O	$\text{K}_2\text{O-Li}_2\text{O}$	
$\text{CuO-Cr}_2\text{O}_3$	$\text{K}_2\text{O-SrO}$	
$\text{CuO-Li}_2\text{O}$	$\text{K}_2\text{S-K}_2\text{CO}_3$	
CuO-MgO	$\text{K}_2\text{SO}_4\text{-NiSO}_4$	
$\text{CuO-Mn}_2\text{O}_3$	$\text{Li}_2\text{O-TiO}_2$	

Ternary systems

new	reassessed	
$\text{Al}_2\text{O}_3\text{-SiO}_2\text{-SrO}$	$\text{Al}_2\text{O}_3\text{-CaF}_2\text{-SiO}_2$	$\text{Al}_2\text{O}_3\text{-NiO-SiO}_2$
$\text{Al}_2\text{O}_3\text{-CuO-SiO}_2$	$\text{Al}_2\text{O}_3\text{-CaO-SiO}_2$	$\text{Al}_2\text{O}_3\text{-P}_2\text{O}_5\text{-SiO}_2$
$\text{Al}_2\text{O}_3\text{-Li}_2\text{O-P}_2\text{O}_5$	$\text{Al}_2\text{O}_3\text{-Cr}_2\text{O}_3\text{-SiO}_2$	$\text{Al}_2\text{O}_3\text{-SiO}_2\text{-TiO}_2$
$\text{Al}_2\text{O}_3\text{-Li}_2\text{O-TiO}_2$	$\text{Al}_2\text{O}_3\text{-Fe}_2\text{O}_3\text{-SiO}_2$	$\text{Al}_2\text{O}_3\text{-SiO}_2\text{-V}_2\text{O}_3$
Ca-Cu-O	$\text{Al}_2\text{O}_3\text{-FeO-SiO}_2$	$\text{Al}_2\text{O}_3\text{-SiO}_2\text{-V}_2\text{O}_5$
$\text{CaO-CaF}_2\text{-P}_2\text{O}_5$	$\text{Al}_2\text{O}_3\text{-K}_2\text{O-SiO}_2$	$\text{Al}_2\text{O}_3\text{-SiO}_2\text{-ZnO}$
Cr-Cu-O	$\text{Al}_2\text{O}_3\text{-Li}_2\text{O-SiO}_2$	$\text{K}_2\text{SO}_4\text{-CaSO}_4\text{-MgSO}_4$
Cu-Li-O	$\text{Al}_2\text{O}_3\text{-MgO-SiO}_2$	$\text{K}_2\text{SO}_4\text{-Na}_2\text{SO}_4\text{-CaSO}_4$
Cu-Mn-O	$\text{Al}_2\text{O}_3\text{-MnO-SiO}_2$	$\text{Na}_2\text{SO}_4\text{-CaSO}_4\text{-MgSO}_4$
$\text{Fe}_2\text{O}_3\text{-SrO-SiO}_2$	$\text{Al}_2\text{O}_3\text{-Na}_2\text{O-SiO}_2$	$\text{Na}_2\text{SO}_4\text{-K}_2\text{SO}_4\text{-MgSO}_4$
$\text{Na}_2\text{CO}_3\text{-K}_2\text{CO}_3\text{-CaCO}_3$		
$\text{Na}_2\text{O-SiO}_2\text{-SrO}$		
SrO-MgO-SiO_2		

Quaternary systems

new	reassessed	
$\text{K}_2\text{CrO}_4\text{-K}_2\text{SO}_4\text{-Na}_2\text{CrO}_4\text{-Na}_2\text{SO}_4$	$\text{Al}_2\text{O}_3\text{-Fe}_2\text{O}_3\text{-K}_2\text{O-SiO}_2$	$\text{Al}_2\text{O}_3\text{-K}_2\text{O-Na}_2\text{O-SiO}_2$
	$\text{Al}_2\text{O}_3\text{-CaO-MgO-SiO}_2$	$\text{Al}_2\text{O}_3\text{-Li}_2\text{O-Na}_2\text{O-SiO}_2$

Contact

In case of questions or to provide feedback, please open a new ticket in our support center: <https://support.gtt-technologies.de/> or contact us via

GTT-Technologies
Kaiserstraße 103
52134 Herzogenrath, Germany
Phone: +49-(0)2407-59533
Fax: +49-(0)2407-59661
E-mail: info@gtt-technologies.de